Investigation of Wagon Derailment Moving on Cable-Stayed Bridge Due to Rail Irregularities

M.M. Jalili[1,*], A.H. Orafa[2], M.T. Ahmadian[3]

[1]Assistant Professor, [2]MSc Student, Department of Mechanical Engineering, Yazd University, [3]Professor, Department of Mechanical Engineering, Sharif University of Technology

jalili@yazduni.ac.ir

Abstract

Rail profile irregularities are one of the main vibration sources to vehicle and track. In this paper derailment of a wagon moving on cable-stayed bridge due to rail irregularities is investigated. The four-axle wagon model is a three-dimensional, non-linear model of a train freight car with 38 DOF. Two parallel rails of the track are modeled as Euler-Bernoulli beams on elastic points as rail pads. The bridge deck is modeled as a plate supported by some cables. Using this model; the effects of wagon specifications, lateral position of the rails and rail irregularities on wagon derailment have been studied.

Keywords: *cable-stayed bridges, Euler-Bernoulli beam, Levy method, Wagon, Derailment*

1. INTRODUCTION

To meet the economic, social and recreational needs of the community for safe and efficient transportation systems, more and more cable bridges have been built throughout the world. The investigation of bridge vibration under moving train using different models has been widely reported in the literature. In most of the previous studies the cable-stayed bridge has been modeled as a planar system. For example Au et al used 2-D model to study bridge vibration due to random rail irregularities [1]. They studied effects of number of random samples, damping, class of railway, track quality and initial motion of train vehicles on bridge vibration. Using a planar vehicle/bridge model, the vibration reduction of cable-stayed bridges subjected to the passage of high-speed trains is studied by Yau and Yang [2]. 2-D models cannot simulate lateral vibration of the bridge. In addition wagon derailment and hunting vibration cannot be investigated by these models.

For the 3-D models, the finite element method has been used as the main tool for bridge simulation. For instance, using FEM, the vibration of coupled train and cable-stayed bridge systems in cross winds has been investigated by Xu et al [3]. Also, the dynamic stability of trains moving over bridges shaken by earthquakes has been studied by Yang and Wu [4]. Using this model the maximum allowable speed for the train to run safely has been obtained under the specified ground acceleration.

In this article, an analytical solution is presented for simulation of the coupled system. A 3-D model of the cable-stayed bridge, rails and freight wagon is developed. Equations of motion of this model are derived. Using the proposed model, the effects of wagon parameters, lateral position of the rails and the rail irregularities on wagon derailment are studied.

2. Brief Review on the Derailment Criteria

One of the criteria for prediction of train derailment is derailment coefficient, which is defined as the ratio of lateral to vertical load at the wheel–rail contact point. The reduction of wheel normal force is also taken as a measure of potential towards derailment in some standards .The limiting values of these parameters differ in different standards. According to the British Standard [5] the limiting values for these parameters are expressed as

$$\begin{cases} \dfrac{Y}{Q} < 1.2 \\ \dfrac{\Delta Q}{Q_0} < 0.6 \end{cases} \tag{1}$$

In Japanese Standard [6], the maximum value of the derailment coefficient is defined as

[Downloaded from uedu.iust.ac.ir on 2025-10-25]

$$\begin{cases} \frac{Y}{Q}=0.8 & \Delta t>0.05s \\ \frac{Y}{Q}=\frac{0.04}{\Delta t} & \Delta t>0.05s \end{cases} \quad (2)$$

In China, the limiting value of Y/Q is 1 [7]. In North America, acceptable performance during the rail cross-level variation test is that the axle sum Y/Q never exceed 1.5, the maximum vehicle body roll angle does not exceed 6◦ peak to peak, and the

Minimum vertical wheel load is never <10 percent of the static wheel load [8].

3. System Model

Figure 1 show the bridge model adopted in the present study. The bridge deck is modeled as a plate supported by some cables. Also the bridge towers are modeled as a beam in lateral and a bar in vertical direction.

Rails are modeled as Euler-Bernoulli beams on elastic points as rail pads (fig 2).

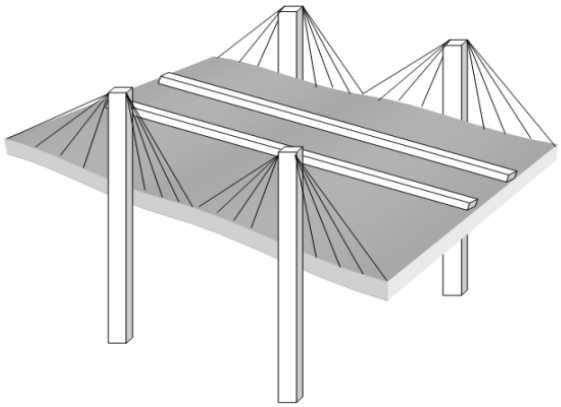

Fig1. 3D model of the bridge

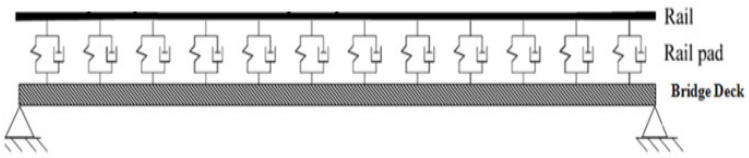

Fig2. Side view of the system model

[Downloaded from uedu.iust.ac.ir on 2025-10-25]

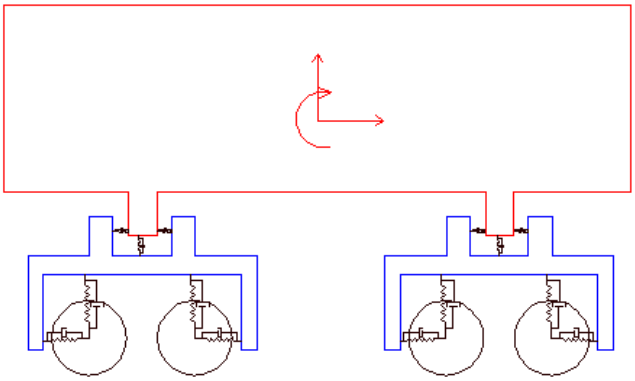

Fig3. Side view of the wagon

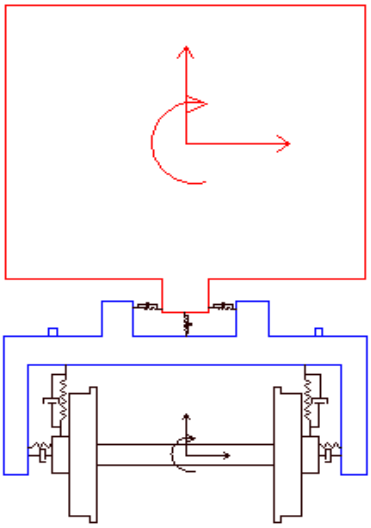

Fig4. Front view of wagon model

Table 1: Degrees of freedom of each part of the wagon

	longitudinal	lateral	vertical	roll	pitch	yaw
Car body	*	*	*	*	*	*
bogie frame	*	*	*	*	*	*
Wheel set	*	*	*	*	*	-

[Downloaded from uedu.iust.ac.ir on 2025-10-25]

4. Equations of Motions:

Deck Equation of Motion:

Describing the bridge deck as a plate, the vertical vibration of the bridge deck is given by:

$$\frac{\partial^4 w_s(x,y,t)}{\partial x^4}+2\frac{\partial^4 w_s(x,y,t)}{\partial x^2\partial y^2}+\frac{\partial^4 w_s(x,y,t)}{\partial y^4}+\frac{\rho_s h_s}{D_s}\frac{\partial^2 w_s(x,y,t)}{\partial t^2}=-\frac{1}{D_s}(F_{ts}^z+\sum_{k=1}^{K}F_{r_k s}) \quad (3)$$

Where:

$$F_{r_k s}=-\sum_{f=1}^{N_f}[K_f(w_s(x_f,y_{r_k},t)-w_{r_k}(x_f,t))+C_f(\dot{w}_s(x_f,y_{r_k},t)-\dot{w}_{r_k}(x_f,t))]\times\delta(x-x_f)\delta(y-y_{r_k}) \quad (4)$$

$$\begin{aligned}F_{ts}^z=&\sum_{c=1}^{N_C}\frac{E_cA_c}{L_c}(C_{11}\delta(y)+C_{33}\delta(y-b))\delta(x-x_c)\sin(\alpha_c)+\\&\sum_{c=N_C+1}^{2N_C}\frac{E_cA_c}{L_c}(C_{21}\delta(y)+C_{43}\delta(y-b))\delta(x-x_c)\sin(\alpha_c)+\\&\sum_{c=2N_C+1}^{3N_C}\frac{E_cA_c}{L_c}(C_{12}\delta(y)+C_{34}\delta(y-b))\delta(x-x_c)\sin(\alpha_c)+\\&\sum_{c=3N_C+1}^{4N_C}\frac{E_cA_c}{L_c}(C_{22}\delta(y)+C_{44}\delta(y-b))\delta(x-x_c)\sin(\alpha_c)\end{aligned} \quad (5)$$

$$\begin{aligned}C_{1k}&=-w_s(x_c,0,t)\sin(\alpha_c)+w_{t_k}^x(H)\cos(\alpha_c)+w_{t_k}^z(H)\sin(\alpha_c)\\C_{2k}&=-w_s(x_c,0,t)\sin(\alpha_c)-w_{t_k}^x(H)\cos(\alpha_c)+w_{t_k}^z(H)\sin(\alpha_c)\\C_{3k}&=-w_s(x_c,b,t)\sin(\alpha_c)+w_{t_k}^x(H)\cos(\alpha_c)+w_{t_k}^z(H)\sin(\alpha_c)\\C_{4k}&=-w_s(x_c,b,t)\sin(\alpha_c)-w_{t_k}^x(H)\cos(\alpha_c)+w_{t_k}^z(H)\sin(\alpha_c)\end{aligned} \quad (6)$$

And

$$D_s=\frac{E_s h_s^{\,3}}{12(1-\nu_s^{\,2})} \quad (7)$$

Using Levy method, the solution of homogenous form of Eq. (3) Can be expressed as [9]:

$$w_s(x,y,t)=X_m(x)Y_{mn}(y)T_{mn}(t)=\sin(\frac{m\pi}{a}x)Y_{mn}(y)T_{mn}(t) \quad (8)$$

Substituting Eq.(8) Into homogenous form of Eq. (3) Yields:

$$[(\frac{m\pi}{a})^4YT-2(\frac{m\pi}{a})^2Y_{mn}^{(2)}T+Y_{mn}^{(4)}T+\frac{\rho_s h_s}{D_s}Y\ddot{T}_{mn}]\sin(\frac{m\pi}{a}x)=0 \quad (9)$$

Using Separation of variables, vibration frequencies can be found as:

$$-\frac{D_s}{\rho_s h_s}[(\frac{m\pi}{a})^4-2(\frac{m\pi}{a})^2\frac{Y_{mn}^{(2)}}{Y_{mn}}+\frac{Y_{mn}^{(4)}}{Y_{mn}}]=\frac{\ddot{T}_{mn}}{T_{mn}}=-\omega_{mn}^{\,2} \quad (10)$$

And finally a differential equation can be derived as follows:

$$Y_{mn}^{(4)}-2(\frac{m\pi}{a})^2Y_{mn}^{(2)}-(\frac{\rho_s h_s}{D_s}\omega_{mn}^{\,2}-(\frac{m\pi}{a})^4)Y_{mn}=0 \quad (11)$$

The bending moments and the shearing forces for the two free edges at y=0 and y=b are equal to zero. So the boundary conditions are:

$$M_y\Big|_{y=0,b}=D_s(\frac{\partial^2 w_s}{\partial y^2}+\nu_s\frac{\partial^2 w_s}{\partial x^2})\Big|_{y=0,b}=D_s(Y_{mn}^{(2)}-\nu_s(\frac{m\pi}{a})^2Y_{mn})\Big|_{y=0,b}=0 \quad (12)$$

$$Q_y\Big|_{y=0,b}=D_s(\frac{\partial^3 w_s}{\partial y^3}+(2-\nu_s)\frac{\partial^3 w_s}{\partial x^2\partial y})\Big|_{y=0,b}=D_s(Y_{mn}^{(3)}-(2-\nu_s)(\frac{m\pi}{a})^2\dot{Y}_{mn})\Big|_{y=0,b}=0 \quad (13)$$

Y_{mn} and ω_{mn} can be achieved by Substituting the solution of Eq.(11) into Eq.(12) and Eq.(13) and solving the obtained homogeneous system.

Solution of Eq.(3) Can be written in the form of Eq.(8). With same X_m and Y_{mn} from homogenous solution. Substituting Eq.(8) Into Eq.(3) Yields:

$$\sum_{m=1}^{N_x}\sum_{n=1}^{N_y}X_m^{(4)}Y_{mn}T_{mn}+2\sum_{m=1}^{N_x}\sum_{n=1}^{N_y}X_m^{(2)}Y_{mn}^{(2)}T_{mn}+\sum_{m=1}^{N_x}\sum_{n=1}^{N_y}X_mY_{mn}^{(4)}T_{mn}+\frac{\rho_s h_s}{D_s}\sum_{m=1}^{N_x}\sum_{n=1}^{N_y}X_mY_{mn}\ddot{T}_{mn}=-\frac{1}{D_s}(F_{ts}^z+\sum_{k=1}^{K}F_{r_k s}) \quad (14)$$

Multiplying Eq.(14) By "$X_k(x)Y_{kh}(y)$" and then applying integral in the plate area yields the second-order ordinary differential equations of the plate vertical vibration in terms of the generalized coordinate $T_{mn}(t)$ as follows:

$$\begin{aligned}&\ddot{T}_{mn}+\frac{D_s}{\rho_s h_s}(\frac{B_3B_2+2B_4B_5+B_1B_6}{B_1B_2})T_{mn}=\\&\frac{1}{\rho_s h_s B_1B_2}(\sum_{c=1}^{N_C}\frac{E_cA_c}{L_c}(C_{11}X_m(x_c)Y_{mn}(0)+C_{33}X_m(x_c)Y_{mn}(b))\sin(\alpha_c)\\&\quad+\sum_{c=N_C+1}^{2N_C}\frac{E_cA_c}{L_c}(C_{21}X_m(x_c)Y(0)+C_{43}X_m(x_c)Y_{mn}(b))\sin(\alpha_c)\\&\quad+\sum_{c=2N_C+1}^{3N_C}\frac{E_cA_c}{L_c}(C_{12}X_m(x_c)Y(0)+C_{34}X_m(x_c)Y_{mn}(b))\sin(\alpha_c)\\&\quad+\sum_{c=3N_C+1}^{4N_C}\frac{E_cA_c}{L_c}(C_{22}X_m(x_c)Y(0)+C_{44}X_m(x_c)Y_{mn}(b))\sin(\alpha_c))\\&\frac{-1}{\rho_s h_s B_1B_2}\sum_{k=1}^{K}\sum_{f=1}^{N_f}[K_f(w_s(x_f,y_{r_k},t)-w_{r_k}(x_f,t))+C_f(\dot{w}_s(x_f,y_{r_k},t)-\dot{w}_{r_k}(x_f,t))]X_m(x_f)Y_{mn}(y_{r_k})\end{aligned} \quad (15)$$

Where

$$\begin{cases}B_1=\int_0^a X_m^{\,2}dx & B_2=\int_0^b Y_{mn}^{\,2}dy & B_3=\int_0^a X_m^{(4)}X_m dx\\B_4=\int_0^a X_m^{\,"}X_m dx & B_5=\int_0^b Y_{mn}^{\,"}Y_{mn}dy & B_6=\int_0^b Y_{mn}^{(4)}Y_{mn}dy\end{cases} \quad (16)$$

5. Tower Equation of Motion:

Describing each tower as an Euler-Bernoulli beam, the lateral vibration of tower is given by:

$$E_tI_t\frac{\partial^4 w_{t_k}^x(x,t)}{\partial x^2}+\rho_tA_t\frac{\partial^2 w_{t_k}^x(x,t)}{\partial t^2}=(F_{tR_k}^x-F_{tL_k}^x) \quad (17)$$

in which

[Downloaded from uedu.iust.ac.ir on 2025-10-25]

$$\begin{cases} F^{x}_{tR_1} = \sum_{c=N_C+1}^{2N_C} \frac{E_c A_c}{L_c} C_{21}\delta(x-H)\cos(\alpha_c) \\ F^{x}_{tR_2} = \sum_{c=3N_C+1}^{4N_C} \frac{E_c A_c}{L_c} C_{22}\delta(x-H)\cos(\alpha_c) \\ F^{x}_{tR_3} = \sum_{c=N_C+1}^{2N_C} \frac{E_c A_c}{L_c} C_{43}\delta(x-H)\cos(\alpha_c) \\ F^{x}_{tR_4} = \sum_{c=3N_C+1}^{4N_C} \frac{E_c A_c}{L_c} C_{44}\delta(x-H)\cos(\alpha_c) \end{cases} \quad (18)$$

and

$$\begin{cases} F^{x}_{tL_1} = \sum_{c=1}^{N_C} \frac{E_c A_c}{L_c} C_{11}\delta(x-H)\cos(\alpha_c) \\ F^{x}_{tL_2} = \sum_{c=N_C+1}^{3N_C} \frac{E_c A_c}{L_c} C_{12}\delta(x-H)\cos(\alpha_c) \\ F^{x}_{tL_3} = \sum_{c=1}^{N_C} \frac{E_c A_c}{L_c} C_{33}\delta(x-H)\cos(\alpha_c) \\ F^{x}_{tL_4} = \sum_{c=N_C+1}^{3N_C} \frac{E_c A_c}{L_c} C_{34}\delta(x-H)\cos(\alpha_c) \end{cases} \quad (19)$$

In order to solve the homogenous form of differential equation in Eq.(17); the solution can be expressed as:

$$w^{x}_{t_k\,l} = X^{x}_{t_k\,l}(x) \times T^{x}_{t_k\,l}(t) \quad (20)$$

where

$$X^{x}_{t_k\,l} = A_1\cos(\beta_l x) + A_2\sin(\beta_l x) + A_3\cosh(\beta_l x) + A_4\sin(\beta_l x) \quad (21)$$

and; the boundary conditions are:

$$\begin{cases} w^{x}_{t_k}(0,t) = 0 \qquad \frac{\partial w^{x}_{t_k}(0,t)}{\partial x} = 0 \\ \frac{\partial^2 w^{x}_{t_k}(H,t)}{\partial x^2} = 0 \quad \frac{\partial^3 w^{x}_{t_k}(H,t)}{\partial x^3} = 0 \end{cases} \quad (22)$$

Using Eq.(20) And boundary conditions; Ai and βl can be found. So; Eq.(17) can be written as follows:

$$E_t I_t X^{x}_{t_k\,l}{}^{(4)} T^{x}_{t_k\,l} + \rho_t A_t X^{x}_{t_k\,l} \ddot{T}^{x}_{t_k\,l} = (F^{x}_{tR_k} - F^{x}_{tL_k}) \quad (23)$$

Using same method as explained in previous section, the second-order ordinary differential equation yields:

$$\ddot{T}^{x}_{t_k\,l} + \frac{E_t I_t \beta_l^4}{\rho_t A_t} T^{x}_{t_k\,l} = \frac{1}{\rho_t A_t B_7} \times$$
$$[(\sum_{c=N_C+1}^{2N_C} \frac{E_c A_c}{L_c} C_{21}\delta(x-H)\cos(\alpha_c)) + \sum_{c=3N_C+1}^{4N_C} \frac{E_c A_c}{L_c} C_{22}\delta(x-H)\cos(\alpha_c)$$
$$+ \sum_{c=N_C+1}^{2N_C} \frac{E_c A_c}{L_c} C_{43}\delta(x-H)\cos(\alpha_c) + \sum_{c=3N_C+1}^{4N_C} \frac{E_c A_c}{L_c} C_{44}\delta(x-H)\cos(\alpha_c))$$
$$-(\sum_{c=1}^{N_C} \frac{E_c A_c}{L_c} C_{11}\delta(x-H)\cos(\alpha_c) + \sum_{c=N_C+1}^{3N_C} \frac{E_c A_c}{L_c} C_{12}\delta(x-H)\cos(\alpha_c)$$
$$+ \sum_{c=1}^{N_C} \frac{E_c A_c}{L_c} C_{33}\delta(x-H)\cos(\alpha_c) + \sum_{c=N_C+1}^{3N_C} \frac{E_c A_c}{L_c} C_{34}\delta(x-H)\cos(\alpha_c))] \quad (24)$$

Where

$$B_7 = \int_0^H X^{2}_{t_k\,l}\, dx \quad (25)$$

For analysis of vertical vibrations of tower, each tower is considered as a bar; so:

$$E_t A_t \frac{\partial^2 w^{z}_{t_k}(x,t)}{\partial x^2} - \rho_t A_t \frac{\partial^2 w^{z}_{t_k}(x,t)}{\partial t^2} = (F^{z}_{tR_k} + F^{z}_{tL_k}) \quad (26)$$

Where

$$\begin{cases} F^{z}_{tR_1} = \sum_{c=N_C+1}^{2N_C} \frac{E_c A_c}{L_c} C_{21}\delta(x-H)\sin(\alpha_c) \\ F^{z}_{tR_2} = \sum_{c=3N_C+1}^{4N_C} \frac{E_c A_c}{L_c} C_{22}\delta(x-H)\sin(\alpha_c) \\ F^{z}_{tR_3} = \sum_{c=N_C+1}^{2N_C} \frac{E_c A_c}{L_c} C_{43}\delta(x-H)\sin(\alpha_c) \\ F^{z}_{tR_4} = \sum_{c=3N_C+1}^{4N_C} \frac{E_c A_c}{L_c} C_{44}\delta(x-H)\sin(\alpha_c) \end{cases} \quad (27)$$

And

$$\begin{cases} F^{z}_{tL_1} = \sum_{c=1}^{N_C} \frac{E_c A_c}{L_c} C_{11}\delta(x-H)\sin(\alpha_c) \\ F^{z}_{tL_2} = \sum_{c=N_C+1}^{3N_C} \frac{E_c A_c}{L_c} C_{12}\delta(x-H)\sin(\alpha_c) \\ F^{z}_{tL_3} = \sum_{c=1}^{N_C} \frac{E_c A_c}{L_c} C_{33}\delta(x-H)\sin(\alpha_c) \\ F^{z}_{tL_4} = \sum_{c=N_C+1}^{3N_C} \frac{E_c A_c}{L_c} C_{34}\delta(x-H)\sin(\alpha_c) \end{cases} \quad (28)$$

The boundary conditions are:

$$\begin{cases} w^{z}_{t_k}(0,t) = 0 \quad , \frac{\partial w^{z}_{t_k}(H,t)}{\partial x} = 0 \end{cases} \quad (29)$$

The solution can be expressed as:

$$w^{z}_{t_k} = \sum_{l=1}^{L} X^{z}_{t_k\,l}(x) T^{z}_{t_k\,l}(t) = \sum_{l=1}^{L} \sin(\frac{(2l-1)\pi}{2H} x) T^{z}_{t_k\,l}(t) \quad (30)$$

Substituting Eq.(30) Into Eq.(26) Yields:

$$[-E_t A_t (\frac{(2l-1)\pi}{2H})^2 T^{z}_{t_k\,l} - \rho_t A_t \ddot{T}^{z}_{t_k\,l}] \sin(\frac{(2l-1)\pi}{2H}) = F^{z}_{tR_k} + F^{z}_{tL_k} \quad (31)$$

Using same approach:

[Downloaded from uedu.iust.ac.ir on 2025-10-25]

$$\ddot{T}^z_{t_k l}+\frac{E_t}{\rho_t}(\frac{(2l-1)\pi}{2H})^2 T^z_{t_k l}=\frac{-1}{\rho_t A_t \frac{H}{2}}\times$$
$$[\sum_{c=N_C+1}^{2N_C}\frac{E_c A_c}{L_c}C_{21}\delta(x-H)\sin(\alpha_c)+\sum_{c=3N_C+1}^{4N_C}\frac{E_c A_c}{L_c}C_{22}\delta(x-H)\sin(\alpha_c)$$
$$+\sum_{c=N_C+1}^{2N_C}\frac{E_c A_c}{L_c}C_{43}\delta(x-H)\sin(\alpha_c)+\sum_{c=3N_C+1}^{4N_C}\frac{E_c A_c}{L_c}C_{44}\delta(x-H)\sin(\alpha_c)$$
$$+\sum_{c=1}^{N_C}\frac{E_c A_c}{L_c}C_{11}\delta(x-H)\sin(\alpha_c)+\sum_{c=N_C+1}^{3N_C}\frac{E_c A_c}{L_c}C_{12}\delta(x-H)\sin(\alpha_c)$$
$$+\sum_{c=1}^{N_C}\frac{E_c A_c}{L_c}C_{33}\delta(x-H)\sin(\alpha_c)+\sum_{c=N_C+1}^{3N_C}\frac{E_c A_c}{L_c}C_{34}\delta(x-H)\sin(\alpha_c)] \quad (32)$$

6. Rail Equation of Motion:

Describing each rail as an Euler-Bernoulli beam, the vertical vibration of rail is given by:

$$E_r I_r\frac{\partial^4 w_{r_k}(x,t)}{\partial x^4}+\rho_r A_r\frac{\partial^2 w_{r_k}(x,t)}{\partial t^2}=F_{s r_k}+F_{w r_k} \quad (33)$$

In which

$$F_{s r_k}=\sum_{f=1}^{N_f}[K_f(w_s(x_f,y_{r_k},t)-w_{r_k}(x_f,t))+C_f(\dot{w}_s(x_f,y_{r_k},t)-\dot{w}_{r_k}(x_f,t))]\delta(x-x_f) \quad (34)$$

$$F_{w r_k}=\sum_{w=1}^{4}F_w^v\,\delta(x-(v_w t+L_w)) \quad (35)$$

The boundary conditions are:

$$\begin{cases} w_{r_k}(0,t)=0 & \dfrac{\partial^2 w_{r_k}(0,t)}{\partial x^2}=0 \\ w_{r_k}(a,t)=0 & \dfrac{\partial^2 w_{r_k}(a,t)}{\partial x^2}=0 \end{cases} \quad (36)$$

The solution can be determined as:

$$w_{r_k}=\sum_{l=1}^{L}X_{r_k l}(x)T_{r_k l}(t)=\sum_{l=1}^{L}\sin(\frac{l\pi}{a}x)T_{r_k l}(t) \quad (37)$$

Substituting Eq.(37) Into Eq.(33) Yields:

$$E_r I_r\sum_{l=1}^{L}X^{(4)}_{r_k l}T_{r_k l}+\rho_r A_r\sum_{l=1}^{L}X_{r_k l}\ddot{T}_{r_k l}=F_{s r_k}+F_{w r_k} \quad (38)$$

The second-order ordinary differential equations of the rail can be found as follows:

$$\ddot{T}_{r_k l}+\frac{E_r I_r}{\rho_r A_r}\frac{B_8}{B_9}T_{r_k l}=\frac{1}{\rho_r A_r B_9}\sum_{w=1}^{4}F_w X_{r_k l}(x-(v_w t+L_w))+\frac{1}{\rho_r A_r B_9}\sum_{f=1}^{N_f}[K_f(w_s(x_f,y_{r_k},t)-w_{r_k}(x_f,t))+C_f(\dot{w}_s(x_f,y_{r_k},t)-\dot{w}_{r_k}(x_f,t))]X_{r_k l}(x_f) \quad (39)$$

$$B_8=\int_0^a X^{(4)}_{r_k l}X_{r_k l}dx=(\frac{l\pi}{a})^4\frac{a}{2}\ ,\quad B_9=\int_0^a X_{r_k l}X_{r_k l}dx=\frac{a}{2} \quad (40)$$

7. Wagon Equation of Motion:

Two coordinate systems are assigned to each part in the wagon model. One fixed to the object center of mass (denoted by r) and rotating with it, and the fixed in space at its center of mass initial position (denoted by o). Also as shown in figure 2 a coordinate system is fixed to the bridge deck as reference.

Using fig.5, the relationship between components of an arbitrary vector in rotating and initial coordinate systems can be given as:

$$R_r^o=R_{x,\varphi}R_{y,\beta}R_{z,\psi}=\begin{bmatrix}1&0&0\\0&\cos\varphi&-\sin\varphi\\0&\sin\varphi&\cos\varphi\end{bmatrix}\begin{bmatrix}\cos\beta&0&\sin\beta\\0&1&0\\-\sin\beta&0&\cos\beta\end{bmatrix}\begin{bmatrix}\cos\psi&-\sin\psi&0\\\sin\psi&\cos\psi&0\\0&0&1\end{bmatrix} \quad (41)$$

Also angular velocity can be obtained as:

$$\begin{aligned}\omega&=\dot{\psi}\hat{k}+\dot{\beta}\hat{j}''+\dot{\varphi}\hat{i}''\\&=\dot{\psi}\hat{k}+\dot{\beta}(\hat{j}\cos\psi+\hat{i}\sin\psi)+\dot{\varphi}(\hat{i}''\cos\beta+\hat{k}''\sin\beta)\\&=\dot{\psi}\hat{k}+\dot{\beta}(\hat{j}\cos\psi+\hat{i}\sin\psi)\\&\quad+\dot{\varphi}(\hat{i}\cos\psi\cos\beta-\hat{j}\sin\psi\cos\beta+\hat{k}\sin\beta)\\&=(\dot{\beta}\sin\psi+\dot{\varphi}\cos\psi\cos\beta)\hat{i}+(\dot{\beta}\cos\psi-\dot{\varphi}\sin\psi\cos\beta)\hat{j}\\&\quad+(\dot{\psi}+\dot{\varphi}\sin\beta)\hat{k}\end{aligned} \quad (42)$$

And angular accelerations are:

$$\begin{cases}\dot{\omega}^x=\ddot{\beta}\sin\psi+\dot{\beta}\dot{\psi}\cos\psi+\ddot{\varphi}\cos\psi\cos\beta-\dot{\varphi}\dot{\beta}\sin\beta\cos\psi\\\qquad-\dot{\varphi}\dot{\psi}\cos\beta\sin\psi\\\dot{\omega}^y=\ddot{\beta}\cos\psi-\dot{\beta}\dot{\psi}\sin\psi-\ddot{\varphi}\sin\psi\cos\beta+\dot{\varphi}\dot{\beta}\sin\beta\sin\psi\\\qquad-\dot{\varphi}\dot{\psi}\cos\beta\cos\psi\\\dot{\omega}^z=\ddot{\psi}+\ddot{\varphi}\sin\beta+\dot{\varphi}\dot{\beta}\cos\beta\end{cases} \quad (43)$$

For each wagon part, the equations of motion can be written as:

$$\sum F=m\ddot{w} \quad (44)$$

$$\sum M^r=\frac{dH^r}{dt}=I^r\dot{\omega}^r+\omega^r\times I\,\omega^r\longrightarrow I^r\dot{\omega}^r=\sum M^r-\omega^r\times I\,\omega^r \quad (45)$$

The summations of the forces and moments applied to the car body are contained wagon body weight, front and rear center plates and side pads forces. The forces and moments of bogies are caused by bogie weight, center plate, side pads and primary suspensions forces. Finally primary suspensions forces, wheelset weight and wheel-rail contact forces cause forces and moments exerted to the wheelset [10,11]

[Downloaded from uedu.iust.ac.ir on 2025-10-25]

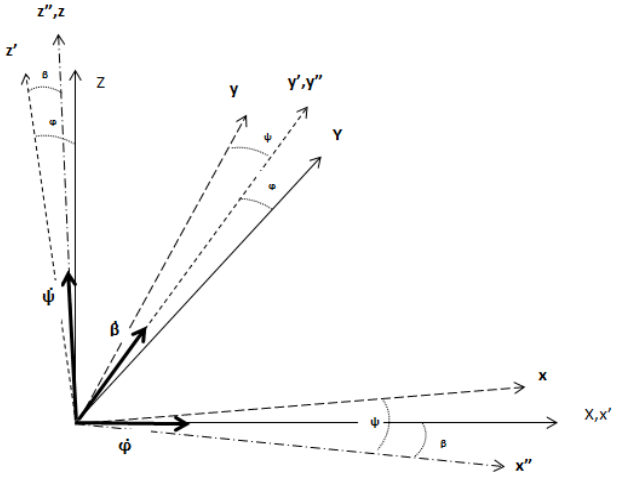

Fig5. Coordinate transformation

8. Irregularities Model:

Rail irregularities generally have a random distribution, and are considered as one of the major source of wagon vibration and wheels derailment. The major causes of these irregularities are: incompatible substrate conditions, whether conditions, rail age and excessive train commutation on rails [12].

The random rail irregularities are assumed to be stationary random and ergodic processes in space, with Gaussian amplitude probability densities and zero mean values. They are characterized by their respective one-sided power spectral density functions $G_{rr}(\omega)$ where ω is the route frequency. Fryba [13] has summarized various commonly used power spectral density functions. In the present study, the power spectral density functions based on the results of measurements on US railway tracks is adopted, with the empirical formula for elevation of irregularities as:

$$G_{rr}(\omega) = \frac{A_v \omega_2^2 (\omega^2 + \omega_1^2)}{\omega^4 (\omega^2 + \omega_2^2)} \tag{46}$$

Where $\omega_1 = 0.0233\, m^{-1}$ and $\omega_2 = 0.131 m^{-1}$ and the parameter A_v is a coefficient related to line grade, as shown in Table 2.

Table 2: Coefficient for Av

Line Grade	A_v	Line Grade	A_v
1	15.52×10^{-8}	4	2.75×10^{-8}
2	8.84×10^{-8}	5	1.55×10^{-8}
3	4.91×10^{-8}	6	0.88×10^{-8}

A sample function of rail irregularities can be generated numerically using the following series:

$$r^d(x) = \sum_{k=1}^{N} a_k \cos(\omega_k x + \varphi_k) \tag{47}$$

Where a_k is the amplitude of the cosine wave, ω_k is a frequency within the interval $[\omega_l, \omega_u]$ in which the power spectral density function is defined, ϕ_k is a random phase angle with uniform probability distribution in the interval $[0, 2\pi]$, x is the global coordinate measured from the start of the rail section and N is the total number of terms used to generate the rail irregularities function. The parameters a_k and ω_k are computed using equations Eq.(48) and Eq.(49):

$$a_k = 2\sqrt{G_{rr}(\omega_k)\Delta\omega} \tag{48}$$

[Downloaded from uedu.iust.ac.ir on 2025-10-25]

$$\omega_k = \omega_l + (k - ½)\Delta\omega \quad (49)$$

$$\Delta\omega = (\omega_u - \omega_l)/N \quad (50)$$

In which ω_u and ω_l are the upper and lower limits of the frequency, and N is a sufficiently large integer. Using equations Eq.(46-50), random rail irregularities in each line grade can be generated. Typical samples of rail irregularities of grade 4 produced by this method is shown in Figure 6.

9. Results and Discussions

To validate the model presented in this paper, its predictions of the responses are compared with the results reported by Au *et al.* [1]. In that reference, the Impact factor of deck moment is obtained using 2D model analyzed by the FEM. The results are compared in figure 7.

It can be seen that there is a close agreement between the simulation results of this research and those of [1].

In order to study the effects of various parameters on wagon derailment, Evripos bridge in Greece is chosen as a case study. The main parameters of the wagon, rails and the bridge used in the simulation are listed in Tables 3-5 [14].

The complete system equations are obtained by combining the equations of motions of deck, towers, rails and the wagon parts. The equations of motion are solved numerically using Runge-Kutta method. The effects of the rail lateral location and wagon specifications on rail vehicle derailment have been illustrated in figures 8-11.

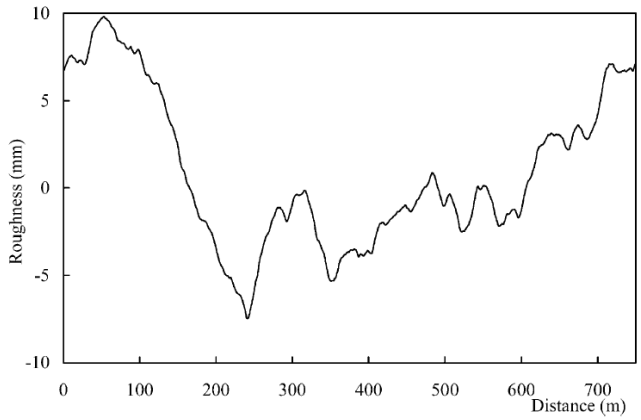

Fig6. Samples of the railway track irregularities [1]

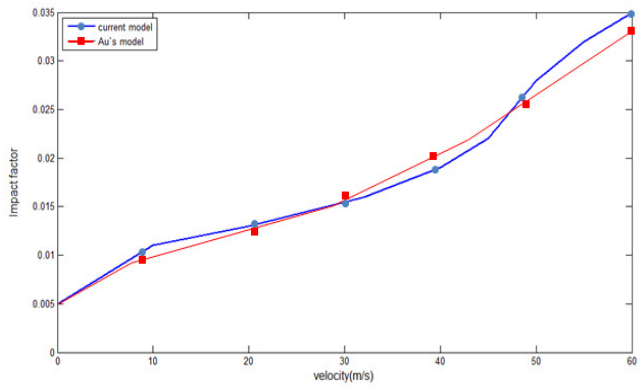

Fig7. Comparison of 2D and 3D model

[Downloaded from uedu.iust.ac.ir on 2025-10-25]

Table 3. Main parameters of wagon

Parameter	Value	Parameter	Value	Parameter	Value
L_w (m)	1.8	m_w (Kg)	1200	I_{bz}(Kg.m^2)	11200
L_b (m)	6.5	I_{bx}(Kg.m^2)	2200	I_{wx}(Kg.m^2)	680
m_b (Kg)	5000	I_{by}(Kg.m^2)	9400	I_{wy}(Kg.m^2)	73

Table 4. Main parameters of rail

Parameter	Value	Parameter	Value	Parameter	Value
E_r (GPa)	205.9	A_r(m2)	7.715×10-3	L_f(m)	0.79
I_r (m4)	3.217×105	K_f(N/m)	6.5×107	L_r(m)	1.5
ρ_r (kg/m3)	7860	C_f(N.s/m)	6.5×104	N_C	10

Table 5. Main parameters of bridge

Parameter	Value	Parameter	Value	Parameter	Value
a(m)	395	$E_{s,t,c}$(GPa)	205.9	H_t (m)	35
b(m)	13.5	$\upsilon_{s,t,c}$	0.29	D_c(inch)	0.6
H_s(m)	0.45	ρ_s(kg/m3)	7860		

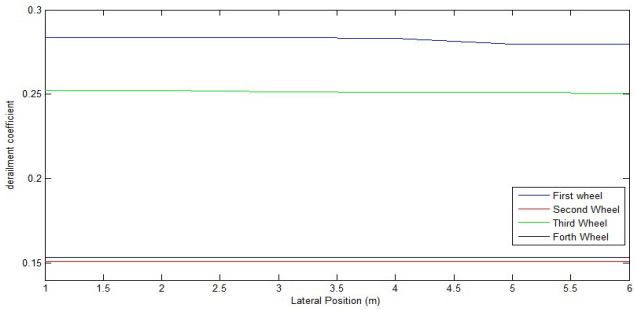

Fig8. Effects of lateral location of rail on bridge deck on derailment coefficient (v=10m/s)

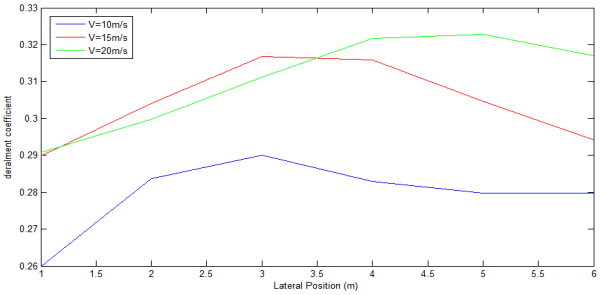

Fig9. Effects of lateral location of rail on bridge deck and wagon velocity on derailment coefficient

[Downloaded from uedu.iust.ac.ir on 2025-10-25]

As illustrated in figure 8, the first wheelset of each bogie has the highest probability of derailment. Figure 9 shows that the derailment coefficient is affected by the lateral position of the rail. It can be seen that, for each velocity, the possibility of wagon derailment is maximum at a particular lateral position. Figures 10-11 show that the derailment risk reduces by increasing the weight of the wagon.

10. Conclusions

In this paper a 3-D nonlinear model is used to investigate derailment of a wagon moving on cable-stayed bridge due to rail irregularities. Using this model; the effects of wagon specifications, lateral position of the rails and rail irregularities on wagon derailment have been studied and following results have been concluded:

The first wheel set of each bogie has the most probability of derailment.

There is an optimum lateral position for wagon in which the possibility of derailment will be minimum. This position is the function of wagon velocity.

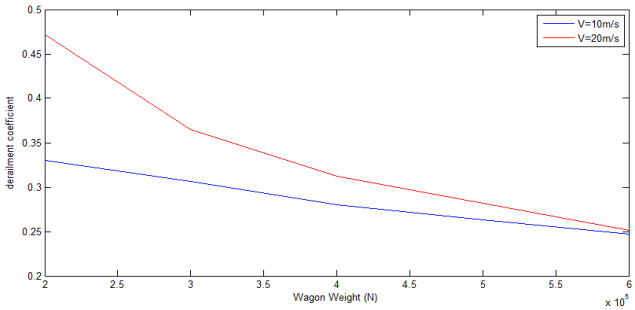

Fig10. Effects of wagon weight on reduction of normal force

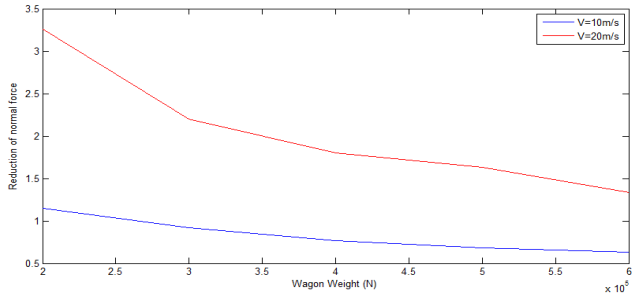

Fig11. Effects of wagon weight on reduction of normal force

References

[1]. Au, F.T.K., Wang, J.J., Cheung, Y.K., "Impact study of cable-stayed railway bridges with random rail irregularities", Engineering Structures, 24, October, pp. 529–541, 2001.

[2]. Yau, J.D., Yang, Y.B., "Vibration reduction for cable-stayed bridges traveled by high-speed trains, "Finite Elements in Analysis and Design, Vol. 40, pp. 341–359, 2004.

[3]. Xu, Y.L., Zhang, N., Xia, H., "Vibration of coupled train and cable-stayed bridge systems in

[Downloaded from uedu.iust.ac.ir on 2025-10-25]

cross winds", Engineering Structures, vol. 26, pp.1389–1406, 2004.
[4]. YANG, Y. B., WU, Y. S., "Dynamic Stability of Trains Moving Over Bridges Shaken by Earthquakes", Journal of Sound and vibration, pp. 65-94, 258(1), 2002.
[5]. Elkins, J. A. and Carter, A., "Testing and Analysis Techniques for Safety Assessment of Rail Vehicles: The State of the Art", Vehicle System Dynamics, Vol. 22, No. 3, pp. 184-208, 1993.
[6]. Jun, X. and Qingyuan, Z., "A Study on Mechanical Mechanism of Train Derailment and Preventive Measures for Derailment", Vehicle System Dynamics, Vol. 43, pp. 121-147, 2005.
[7]. Matsuura, A., "Dynamic Interaction of Vehicle and Track", Quarterly Report of RTRI, Vol. 33, No. 1, pp. 31-38, 1992.
[8]. Elkins, J. A. and Carter, A. Testing and analysis techniques for safety assessment of rail vehicles: the state of-the-art.Veh. Syst. Dyn, 22, pp.185–208, 1993.
[9]. Xiang, Y., Zhao, Y.B., Wei, G.W., "Levy solutions for vibration of multi-span rectangular plates", International Journal of Mechanical Sciences 44, pp. 1195–1218, 2002.
[10]. Garg, V. K., and Dukkipati, R. V., "Dynamics of Railway Vehicle Systems", Academic Press, Canada, 1984.
[11]. Durali, M. and Shadmehri, B., "Nonlinear Analysis of Train Derailment in Severe Braking", Journal of Dynamic Systems, Measurement, and Control, Vol. 125, pp. 48-53, 2003.
[12]. Iyengar, R.N. and Jaiswal, O. R., "Random Field Modeling of Railway Track Irregularites", Journal of Transportation Engineering, pp. 303-308, 1995.
[13]. Fryba L. "Dynamics of railway bridges", London: Thomas Telford, 1996.
[14]. Virlogeux, M., "Recent evolution of cable-stayed bridges", Engineering Structures 21, pp. 737–755, 1999.

[Downloaded from uedu.iust.ac.ir on 2025-10-25]

List of Symbols

A	Cross section area	α	Geometric slope
C	Fastener damping in vertical direction	υ	Poisson's ratio
D	Flexural rigidity	ρ	Density
E	Module of elasticity	ω	Angular velocity
F	Force	$(\ )^r$	Relative frame
H	Tower height	$(\ )^x$	Horizontal direction
I	Second moment of area	$(\ )^y$	Lateral direction
K	Fastener stiffness in vertical direction	$(\ )^z$	Vertical direction
L	Length or distance between different elements	$(\ )_b$	bogie
N	Number of.	$(\ )_c$	C^{th} cable
a	Bridge length	$(\ )_f$	F^{th} fastener
b	Bridge width	$(\ )_k$	K^{th} rail or tower
d	Diameter of.	$(\ )_o$	Initial frame
h	Deck thickness	$(\ )_r$	Rail
m	Mass	$(\ )_{tR}$	Right side of tower
v	Velocity	$(\ )_{rs}$	Rail to bridge deck
w	Displacement	$(\ )_{rw}$	Rail to wheel
$(\ )_s$	Bridge deck	$(\ )_{ts}$	Tower to bridge deck
$(\ )_{sr}$	Bridge deck to rail	$(\ )_w$	W^{th} wheel set
$(\ )_{st}$	Bridge deck to tower	$(\ )_{wg}$	Wagon
$(\ )_t$	Tower	$(\ )_{wr}$	Wheel to rail
$(\ )_{tL}$	Left side of tower		

[Downloaded from uedu.iust.ac.ir on 2025-10-25]